RETRACING (AND RE-RAYTRACING) AMUNDSEN'S JOURNEY THROUGH THE NORTHWEST PASSAGE

Beaudoin, J.D.[1], Hughes Clarke, J.E.[1], and Bartlett, J.E.[2]

1: Ocean Mapping Group (OMG), University of New Brunswick, Fredericton, New Brunswick

2: Canadian Hydrographic Service, Burlington, Ontario

ABSTRACT

The accuracy of a multibeam survey depends directly on our knowledge of the sound speed, both at the transducer face and throughout the watercolumn. Uncertainties in either case lead directly to systematic errors in the depth and positioning of soundings. In the ideal situation, both quantities are measured with sufficient temporal and spatial resolution such that their effects are adequately accounted for. This is not always the case, however, and the hydrographer may need to apply new sound speed information in post-processing. This involves re-pointing the beam launch vector given new surface sound speed information and/or re-raytracing using new sound speed profile information.

Such was the case on the CCGS Amundsen while transiting the Northwest Passage in the autumn of 2003 with a fresh Simrad EM300 installation. Sound speed profiles were often collected after the fact; further complicating this was the occasional failure of the pump that supplied a constant flow of water to the surface sound speed probe. Though re-raytracing soundings is a straightforward procedure with the EM300, many challenges arise in determining the beam geometry if one is required to re-point the beam vector given new surface sound speed information. Difficulties arise from: (1) sector timings and boundaries changing with operational mode (e.g. shallow vs. deep), and (2) insufficient information to determine the transmit sector associated with a receive beam.

It is the intent of this paper to present a systematic approach to solving this type of problem. Theoretical examples from selected multibeam sonars are presented with practical examples focusing on the EM300 as installed on the CCGS Amundsen.

INTRODUCTION

The accuracy of a multibeam survey depends directly on our knowledge of the sound speed, both at the transducer face and throughout the watercolumn. Uncertainties in either case lead directly to systematic errors in the depth and positioning of soundings. In the ideal situation, both quantities are measured with sufficient temporal and spatial resolution such that their effects are adequately accounted for. This is not always the case, however, and the hydrographer may need to apply new sound speed information in post-processing. This involves adjusting the beam launch vector given new surface sound speed information and/or re-raytracing using new sound speed profile information. During an autumn transit of the Northwest Passage in 2003, the CCGS Amundsen collected swath bathymetry throughout the Passage and also during oceanographic mooring operations in the Beaufort Sea (refer to Figure 1). Lack of sound speed profile collection and failure of the surface sound speed probe led to an extensive amount of post-processing to minimize systematic biases due to sound speed errors. It is the intent of this paper to document the approach taken for the application of sound speed information in post-processing for the Amundsen's EM300 and pass on experience garnered from working on similar problems with other multibeam systems.

The CCGS Amundsen (formerly Sir John Franklin) is a 98-meter 1200 class icebreaker completely rigged for various scientific activities and capable of extended stays in the Arctic. The vessel is equipped with a Kongsberg-Simrad EM300, which is a shallow to mid ocean depth system (nominally 10m - 5000m) with a nominal frequency of 30 kHz. The transmit fan is split into several frequency-coded sectors ranging from 27 -34 kHz, with the number of sectors varying from three to nine depending on the operating mode (which is depth dependant). These sectors are transmitted sequentially at each ping which leads to complications during the determination of vessel orientation at transmit and receive times, as will be shown later.

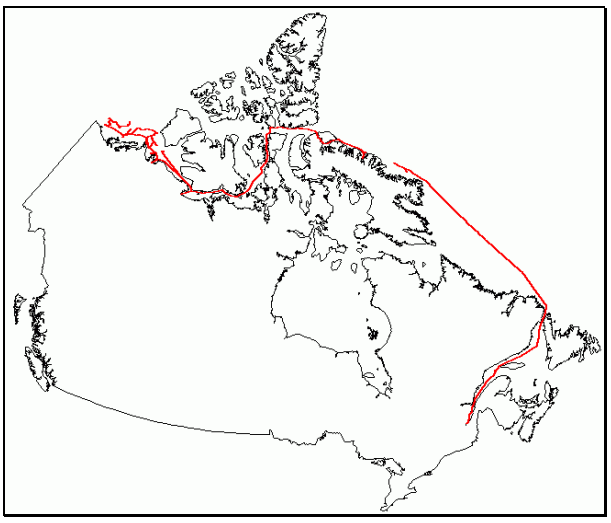

Figure 1. Ship track of CCGS Amundsen, September 2003, departing from Quebec City.

The vessel was equipped with a hull-mounted sound speed probe that provided real-time transducer surface sound speed to the transceiver to ensure correct beam steering. For sound speed throughout the water column, the vessel was equipped with a Brooke Ocean Technology MVP-300 (Moving Vessel Profiler) that was capable of being towed behind the vessel, collecting water column information along the vessel track through a repetitive freefall dipping motion. In the ideal situation, the sensor would be deployed at all times during a survey and the water column information applied immediately (thus little sound speed profile would be required in post-processing).

The reality of the first transit operations was that the crew was concerned for the safety of the MVP system, this concern being aggravated by the intermittent ice cover throughout the Passage. However, a secondary issue became a critical factor: as the system was fitted with a glass conductivity cell (part of a Seabird 911 CTD), it could not be allowed to fill with the fresh water commonly found at the sea surface otherwise it would freeze and destroy the sensor. This limited the use of underway MVP operations, as such the only sound speed profiles were obtained when a CTD rosette cast was performed at the location of an oceanographic mooring deployment. This yielded approximately a single profile per day in the western Arctic; however, no profiles were collected at all during the transit of the Northwest Passage. In addition to the lack of sound speed profiles, the pump that supplied the surface sound speed probe would occasionally fail.

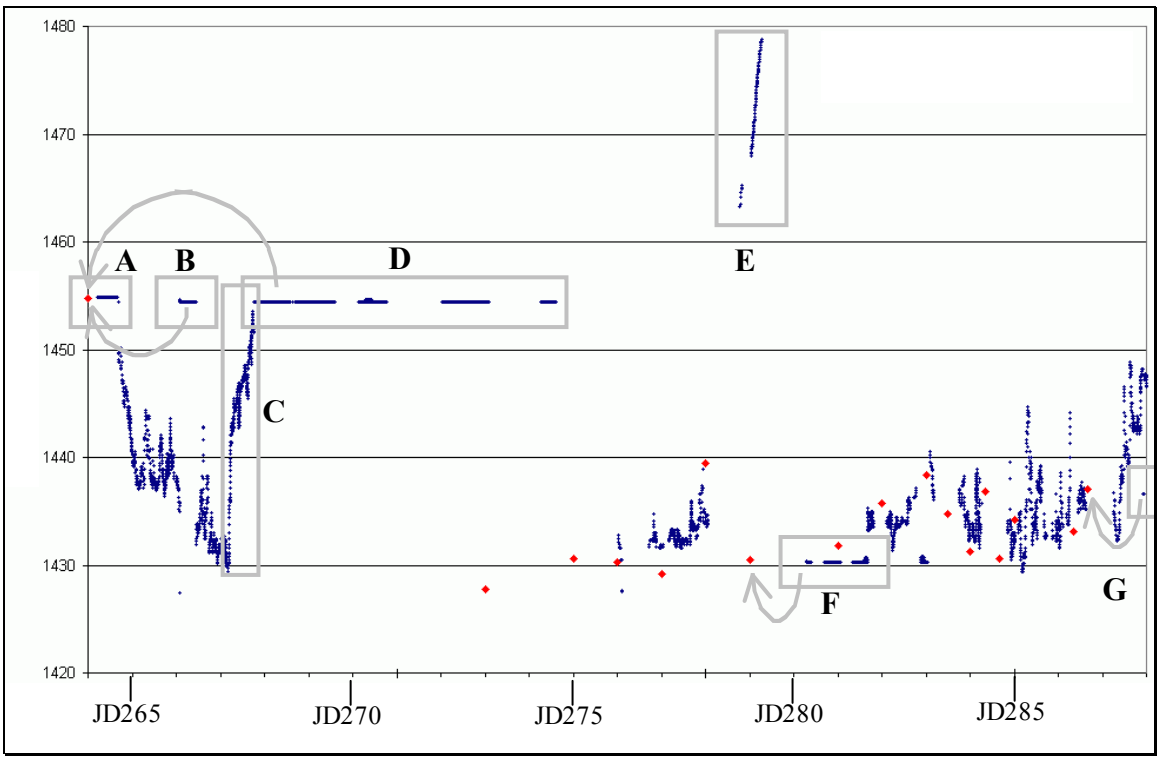

Figure 2. Time-series plot of surface sound speed measured throughout the cruise. Red points signify sound speed measured from a sound speed profile, blue points represent the sound speed used by the transceiver in beam steering calculations; this value is either taken from a real-time probe on the hull or from the last sound speed profile (or from an operator specified value, though this option was never exercised). Time-axis is labeled in Julian days; vertical axis is sound speed in meters per second.

Plots of the surface sound speed used in beam steering calculations have been prepared and are shown in Figure 2 (the same data area mapped geographically in Figure 3). Surface sound speeds range from 1450 m/s near Baffin Island to 1430-1440 m/s throughout the archipelago and in the Beaufort Sea (refer to Figure 3). Several artifacts can be noted in the raw data; for example, Section E demonstrates the effect of an unnoticed (or overnight) pump failure with a steady rise in sound speed until the failure was noticed. Until the operator noticed the failure, the water in the probe heated to inner hull temperatures and artificially raised the sound speed. In that case, the operator chose to use the sound speed from the last collected sound profile as an approximation of the true surface sound speed (as shown by the grey arrows in Figure 2), leading to the flat-line sound speed observations in F. Similar flat line events occur in A, B, D, and G. In all cases, the sound speed used for beam steering was taken from the last sound profile

and the surface sound speed probe data were ignored (whether the data were acceptable or not). The particulars of each section are summarized in Table 1 and are further discussed on an individual basis in the section dealing with the practical application of the methodology.

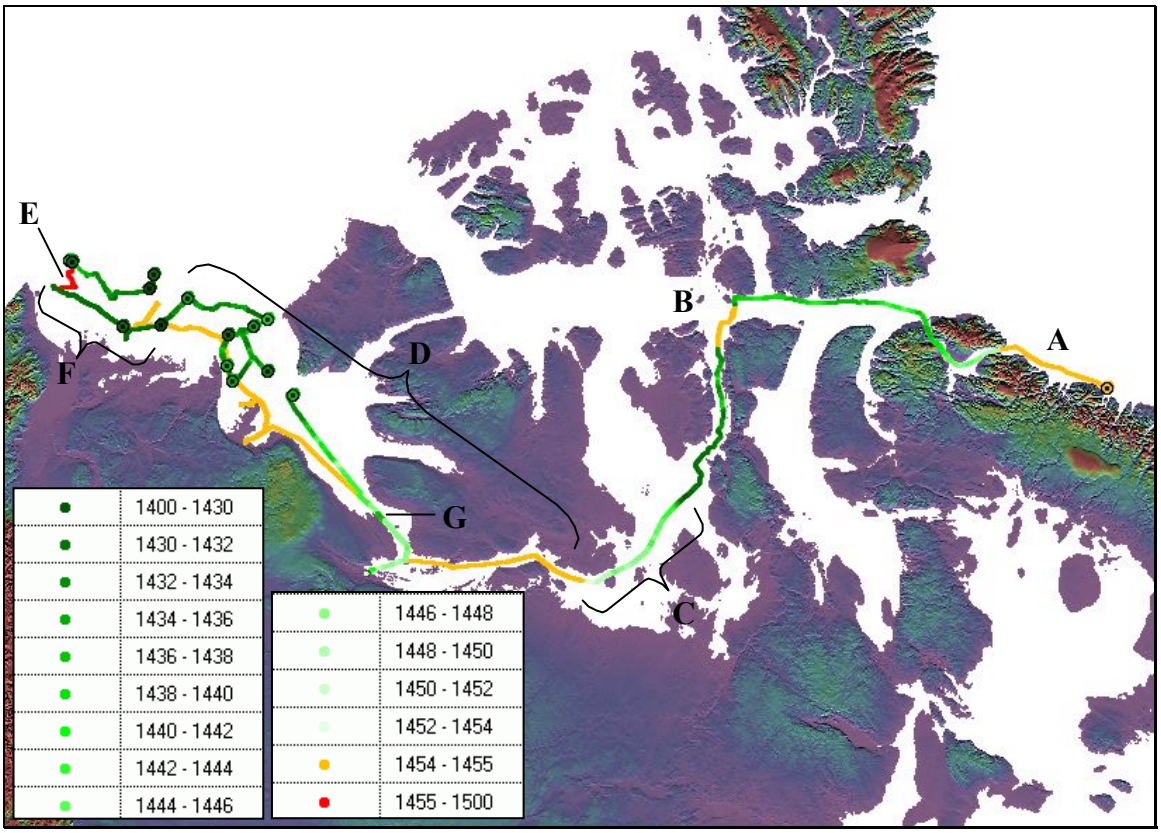

Figure 3. Map of surface sound speed collected during transit through the Arctic Archipelago. Event labels correspond to those of Figure 2. Note that western return leg coming through Dolphin and Union Strait overlaps outward leg of transit (in yellow, near event G). Dotted locations represent approximate location of collected sound speed profiles, with colours corresponding to sound speed at transducer depth.

Table 1. Explanation of observed surface sound speed artifacts.

Artifact	Explanation
A	Surface sound speed probe inoperative, no data logged, speed interpolated from watercolumn.
B	Surface sound speed probe inoperative, no data logged, speed interpolated from watercolumn.
C	Surface sound speed pump appears to have failed.

D	Surface sound speed probe operative but data not used, speed interpolated from watercolumn.
E	Surface sound speed pump confirmed to have failed.
F	Surface sound speed probe operative but data not used, speed interpolated from watercolumn.
G	Surface sound speed probe operative but data not used, speed interpolated from watercolumn.

POST-PROCESSING METHODOLOGY

Faced with grossly erroneous surface sound speed values, incorrect soundings may be corrected based on an estimate of the correct surface sound speed as long as the following data are preserved in the raw data stream [Hughes Clarke et al., 2000]:

1. Array relative steering angles.
2. Full resolution orientation time series.
3. Lever arms between all sensors, and alignment angles.
4. Sound speed applied in beam steering process.

For example, the surface sound speeds in Section A (Figure 2) can be linearly interpolated between 1455 m/s and 1450 m/s. After the recalculation of the beam steering angles, the orientation can then be re-applied to compute the new beam launch angle, followed by a raytrace using the appropriate sound speed profile. The sound speed profile can be linearly interpolated in the western portions of the survey where the relatively high frequency of profile collection justifies such an approach [Hughes Clarke et al., 2000].

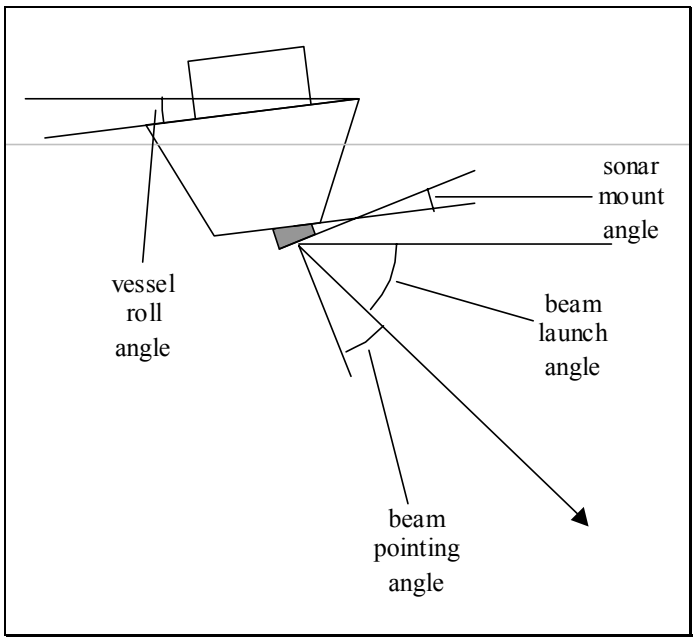

Figure 4. Illustration of difference between beam-pointing angle and beam launch angle. The beam-pointing angle is relative to the transducer boresite whereas the beam launch angle is referenced to the local vertical and accounts for effects due to vessel orientation and mount angles. Note that pitch and yaw are ignored in this illustration though they play a potentially significant role in the determination of beam launch angle. The beam-pointing angle is corrected during the beam re-pointing procedure outlined in this work.

In the general case, one must begin with the fundamental measurements made by the sonar, i.e. range and steering angle, and re-point the original array-relative steering angle if necessary (beam-pointing angle in Figure 4). The next step is to recreate the sounding geometry at transmit and receive in order to determine the beam's geographic launch vector (beam launch angle in Figure 4). Having done this, an acoustic raytrace provides the depth and horizontal range with the beam azimuth being used to reduce the horizontal measurement into across-track and along-track components. Finally, the lever arms between the reference point and the transducer are rotated using the transmit orientation, and are then added to the depth, across-track and along-track offsets to yield the sounding solution with respect to the reference point. The above boils down to a four-step process:

1. Re-compute beam pointing vector.
2. Determine geographic launch vector.
3. Perform raytrace.
4. Reduce to vessel reference point.

Presented with new surface or watercolumn sound speed information in post-processing, the procedure varies only in the entry point of the four-step process above.

Three scenarios exist with the entry point for each case summarized in Table 2, with each step discussed further below.

Table 2. Application of new sound speed information for an electronically steered array.

Surface Sound Speed	Sound Speed Profile	Entry Point
New value	New profile	Step 1
New value	Acceptable profile	Step 1
Acceptable value	New profile	Step 3

This work is based on experience garnered while attempting to deal with sound speed and orientation problems for a range of sonars requiring post-processing at various stages of the procedure outlined in this document. Examples include:

1. RV Heron, (Shippigan, New Brunswick, 2003): Primary motion sensor data was faulty, EM3000 beam launch vector had to be recomputed using secondary motion sensor data.
2. Snellius Ship Acceptance Trials, Royal Netherlands Navy (Netherlands, 2003): Surface sound speed logged externally, thus EM3000D beam pointing vector had to be adjusted in post-processing.
3. CCGS Vector (2003): Re-computation of EM1002 beam launch vector due to delay in orientation time series.

Step 1: Re-compute beam pointing vector

Multibeam sonars rely on the principle of electronic beam steering to direct the main response axis (MRA) of the transmitter and receiver arrays. Both arrays typically consist of a series of acoustic elements, with the signals from all elements being summed to focus the response pattern of the array into a narrow beam. Beam steering, or the redirection of the MRA, is achieved through the addition of time or phase delays during the element summation process. The process of adding time or phase delays requires knowledge of the speed of sound at the array face since phase and time delays are based upon the wavelength associated with the sonar's operating frequency. Errors in the knowledge of surface sound speed lead directly to systematic errors in beam pointing

angles through the calculation of wavelength based on sound speed. These errors grow proportionally to steering angle, thus the largest error is encountered in the outer beams of a steered linear array whereas the accuracy of beams near nadir suffers little, as shown in Figure 5 [Hughes Clarke, 2003].

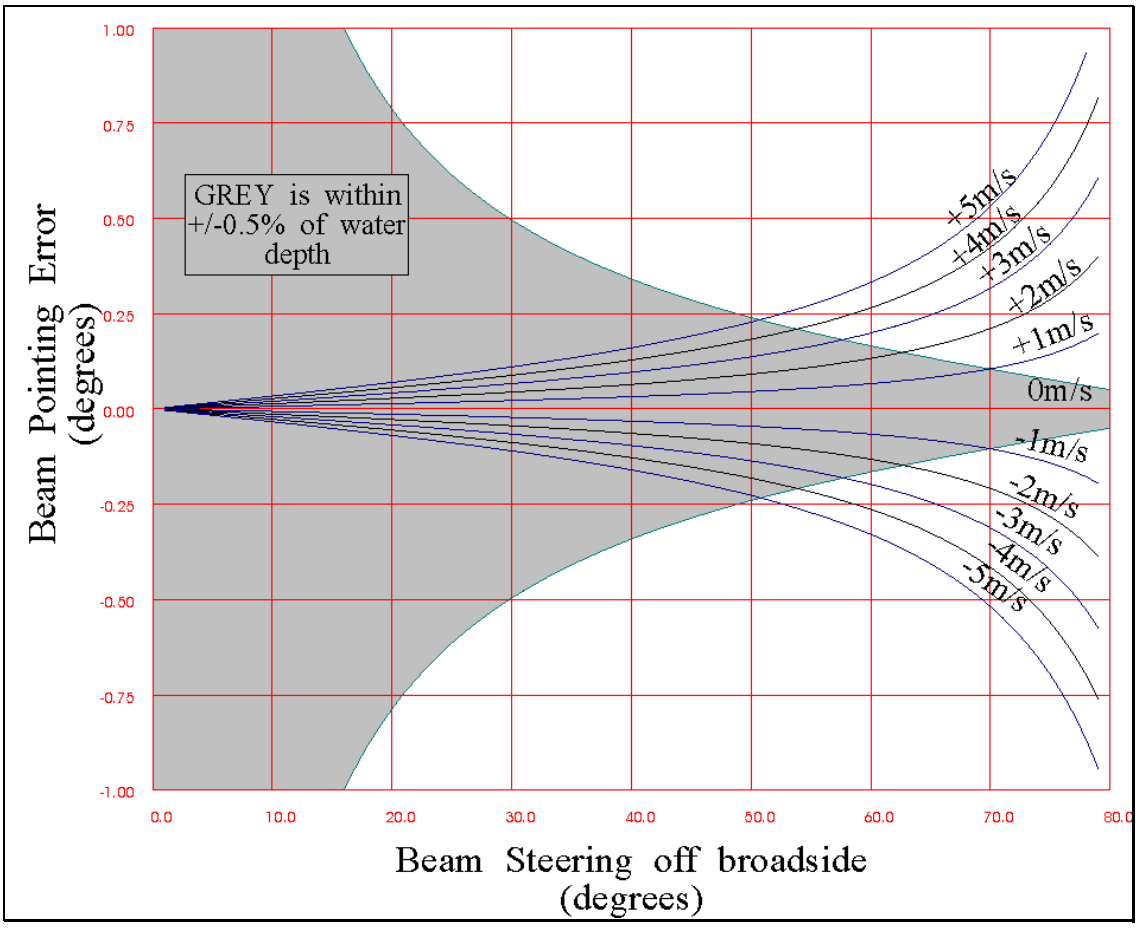

Figure 5. Linear array beam steering sensitivity to surface sound speed error [after Hughes Clarke, 2003]. Clearly, even small errors in surface sound speed can degrade the accuracy of depth solutions associated with outer beams.

Procedure & Application

Re-pointing a beam involves computing a new array-relative steering angle based on the new sound speed and original steering angle and sound speed. Snell's Law relates the four values:

$$\frac{s_1}{\sin\theta_1} = \frac{s_2}{\sin\theta_2} \qquad (1)$$

Given sound speeds s_1 and s_2 and the original array-relative steering angle θ_1, we solve for the new steering angle as such:

$$\theta_2 = \sin^{-1}\left(\frac{s_2}{s_1}\cdot \sin\theta_1\right) \qquad (2)$$

The concept of re-pointing beam steering angles was successfully put into practice during a sea acceptance trial of the Snellius, a Royal Netherlands Navy hydrographic survey ship. Equipped with an EM3000D, the data were captured and logged using QINSy. The surface sound speed probe was not interfaced with the EM3000D transceiver unit; instead it was logged separately, with the operator occasionally updating the value. The correct sound speed was later incorporated during post-processing using the methodology presented in this paper. Sun-illuminated digital terrain models (DTM) were generated prior to and following the application of the surface sound speed in post-processing, with a subset of the results being shown in Figure 6.

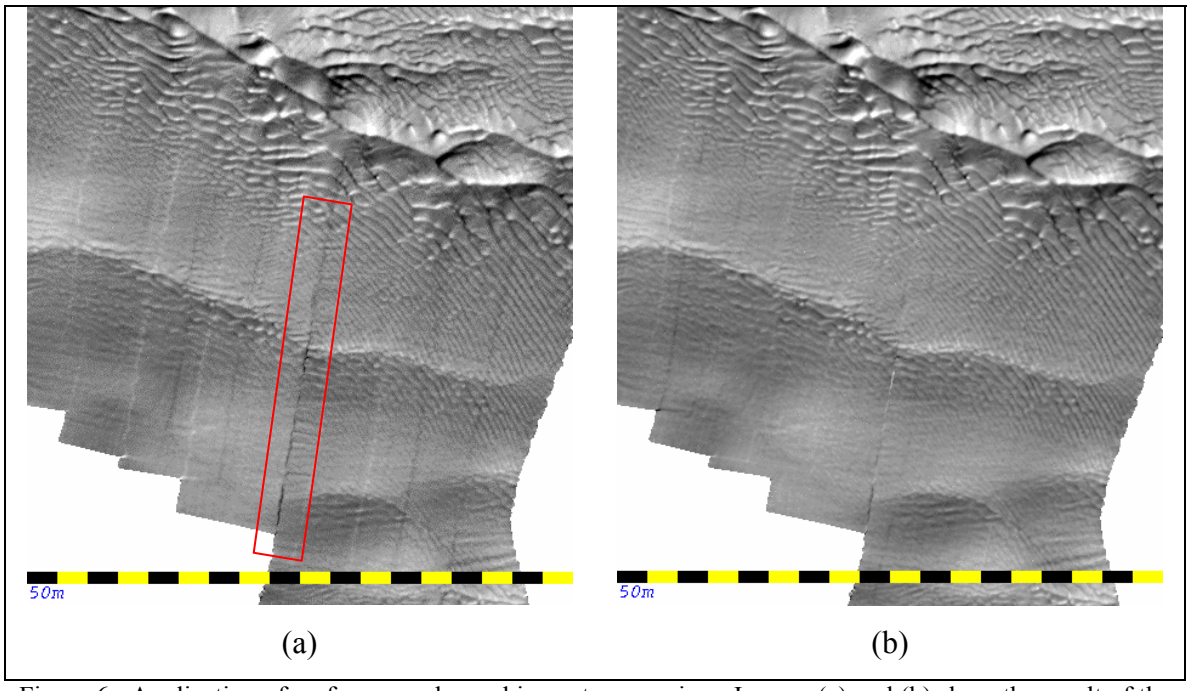

Figure 6. Application of surface sound speed in post-processing. Images (a) and (b) show the result of the application of surface sound speed information in post-processing with (a) representing the raw data whereas (b) has been corrected for surface sound speed errors. Ship tracks run roughly north-south; gridding artifacts are introduced in areas of overlap between adjacent survey lines (highlighted in red in (a)). Residual artifacts in (b) are due to incorrect tidal modeling.

The images in Figure 6 demonstrate the successful re-pointing of beams when the surface sound speed is *slightly* in error; however, it is useful to see the effect of a grossly incorrect sound speed. To this end, an additional line was collected at the end of the survey with the operator intentionally setting an incorrect surface sound speed of 1550 m/s (the actual sound speed was approximately 1480 m/s). A subset of the soundings from this line are plotted against a DTM created from the survey data in Figure 7, showing the raw soundings and the re-pointed soundings as red and black crosses, respectively (the DTM is shown as solid black lines). One may thus conclude that the beam re-pointing methodology functions well, even in the event of gross errors in the original estimation of the surface sound speed.

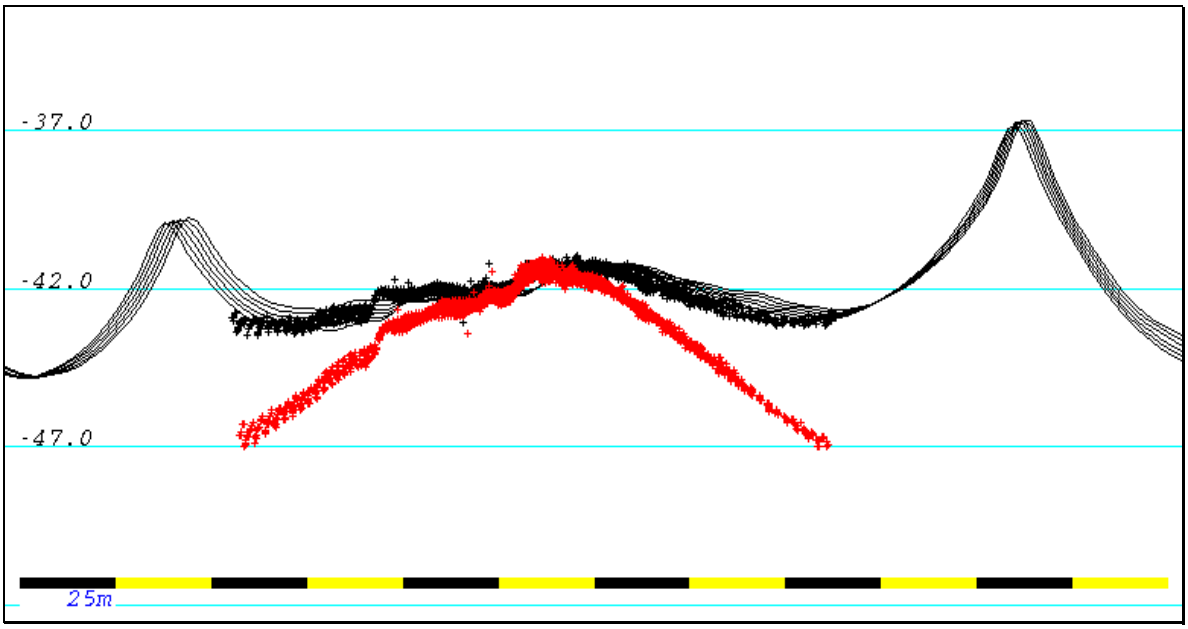

Figure 7. Effect of gross error in surface sound speed. An additional survey line was run with an intentionally incorrect surface sound speed, depicted by the red soundings in the cross-sections on the right. The black soundings have been corrected in post-processing using the sound speed value provided by the sensor. Solid black lines represent data from DTM shown in Figure 6(b). Note the close agreement between corrected soundings (black crosses) and the underlying DTM.

Complications

Re-pointing of beams is applicable both on transmit and receive arrays, but *only* if they are steered arrays. An example best illustrates the point. The RESON SeaBat 8101 and 8111 use linear arrays on transmit and arcuate (barrel) arrays on receive. Beam re-

pointing is meaningless on receive since the surface sound speed has no impact on the beam pointing angle, this being the main advantage of using an arcuate receive array. The transmit arrays, on the other hand, are linear and potentially pitch stabilized. If pitch stabilization is not used, then the transmit beam is not steered and no re-pointing is necessary. However, if pitch stabilization is used, the transmitter steering angle may be re-pointed given new surface sound speed information.

Some arcuate receive arrays must electronically steer their outermost receive beams to achieve their full angular sector. In the case of the EM1002, this occurs at +/- 50º from the center of the receive array, as shown in Figure 8. The raw data telegram reports the beam angle from the center of the array, thus one must take care to remove 50º from the reported angle in the event that re-pointing is required, e.g. a beam with a reported steering angle of 53º is physically mounted at 50º and steered an additional 3º.

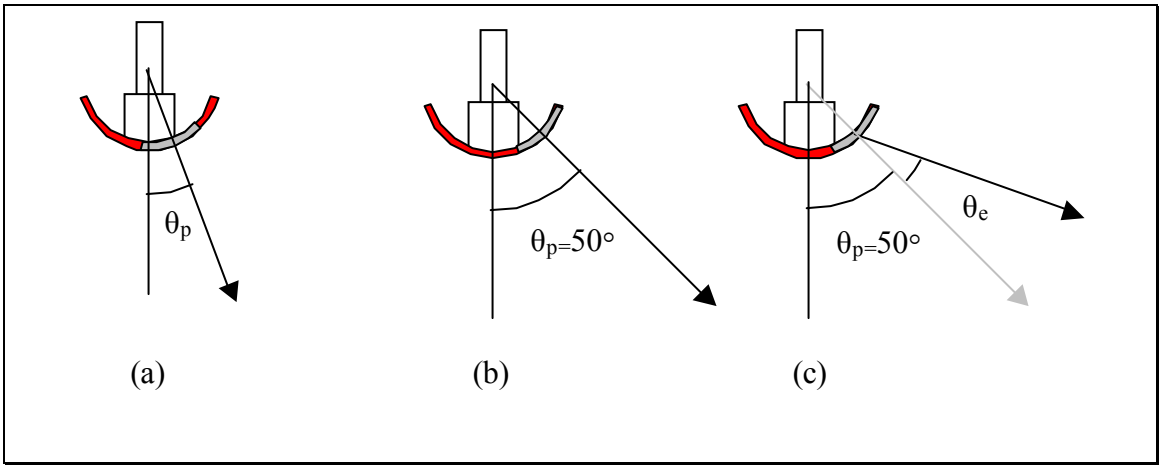

Figure 8. Beam steering of outer beams with an arcuate receiver array. For any given receive beam, only a subset of the receiver arc is used in beamforming, shown as the grey portion in (a). In this case, the receive beam is physically steered to θ_p. Image (b) demonstrates the last furthest achievable receive beam (since a subset cannot be created past the edge of the arc). In the case where further angular coverage is desired, as in (c), one must introducing an additional electronic steering angle, θ_e.

Step 2: Determine geographic launch vector

In general, fourteen angles are required to determine a sounding's geographic pointing vector, consisting of four roll, pitch and heading triplets and two steering angles:

(1) Orientations at time of transmit and receive (6 angles).

(2) Transmitter and receiver mounting angles (6 angles).

(3) Steering angle on transmit and receive (2 angles).

The orientations at the times of transmit and receive are ascertained by determining the times of both events and then interpolating the orientation using the orientation time-series values before and after each time. The transmit time is recorded with the bathymetry packet whereas the receive time is computed through the addition of the transmit time and the two-way travel-time for each receive beam. The mount angles are determined during a patch test or vessel installation survey. It is important to note that some sonars share the same mount angles for the transmitter and receiver as they are installed as a single physical unit (and assuming perfect orientation within the transducer). At this point, it is necessary to discuss the vessel coordinate system that is used in this work. The coordinate system is right-handed with the positive x-axis pointing towards the bow, the positive y-axis pointing towards starboard and the positive z-axis pointing below the vessel. The sign convention for angular measurements follows the right hand rule, i.e. positive roll is to starboard (starboard sinks, port rises), positive pitch is nose-up (bow rises, stern sinks), and positive yaw is clockwise (bow turns to starboard). All rotations are applied in the order of roll, pitch, and finally heading.

Given the necessary angular measurements, the next step is to determine where the transmitter and receiver were pointing in space at the transmit and receive times. These vectors are then used to build a coordinate system from which the beam's pointing vector can be determined using the transmit and receive steering angles. The beam-pointing vector is then referenced to the local level coordinate system.

The procedure begins with an ideal transmit unit vector pointing perfectly along the ship's x-axis, i.e. (1,0,0). This ideal vector is then rotated using the transmitter alignment angles, immediately followed by the orientation of the transmitter at transmit time, as in (1). The same is done in (2) for the receiver with its mount angles and orientation; however, the ideal receiver vector is oriented perfectly with the ship's y-axis, i.e. (0,1,0). Note that the rotation matrices in (3) and (4) are composed of three individual rotation matrices that represent roll, pitch, and heading (must rotate in this order).

$$\overrightarrow{TX} = R_{orientation} \cdot R_{alignment} \cdot \overrightarrow{TX}_{ideal} \qquad (3)$$

$$\overrightarrow{RX} = R_{orientation} \cdot R_{alignment} \cdot \overrightarrow{RX}_{ideal} \quad (4)$$

The vectors *TX* and *RX* represent the orientation of the transmitter and receiver at the times of transmit and receive, respectively, in the locally level coordinate system.

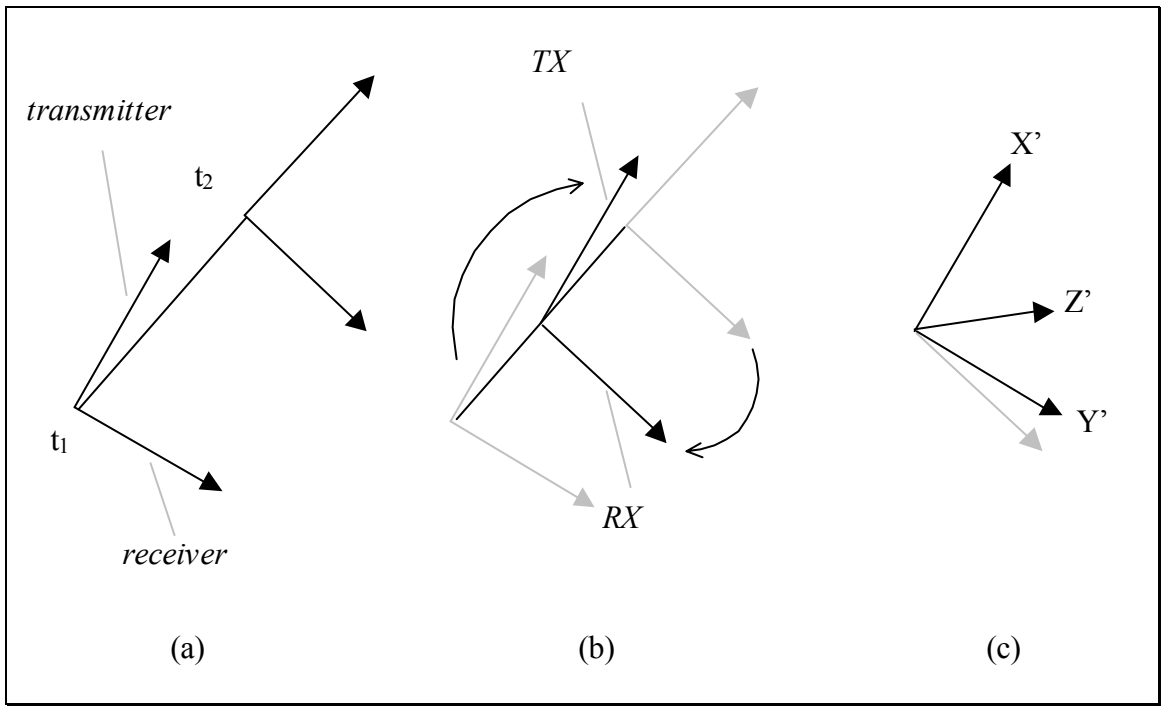

Figure 9. Construction of beam vector coordinate system. The orientation of the transmitter/receiver assembly changes from the time of transmit and receive, represented by t_1 and t_2, respectively, in (a). The transmit vector (*TX*) and the receiver vector (*RX*) are then migrated to the midpoint between the two positions, as in (b). A coordinate system is then built in which *TX* is the x-axis, the z-axis is orthogonal to the plane containing *TX* and *RX* and the y-axis is orthogonal to the x-axis and z-axis (depicted in (c)). It is in this coordinate system that the beam-pointing vector is computed.

Figure 9 depicts how these two vectors are then used to build a coordinate system in which the beam-pointing vector can be measured. This coordinate system is created through the use of the cross product:

$$\overrightarrow{X'} = \overrightarrow{TX} \quad (5)$$

$$\overrightarrow{Z'} = \overrightarrow{TX} \times \overrightarrow{RX} \quad (6)$$

$$\overrightarrow{Y'} = \overrightarrow{Z'} \times \overrightarrow{X'} \quad (7)$$

The beam-pointing vector is then computed in this coordinate system through the following equations, as depicted in Figure 10:

$$\delta = \cos^{-1}(\overrightarrow{TX} \cdot \overrightarrow{RX}) - \frac{\pi}{2} \tag{8}$$

$$y_1 = \frac{\sin(RX_{steer})}{\cos(\delta)} \tag{9}$$

$$y_2 = \sin(TX_{steer}) \cdot \tan(\delta) \tag{10}$$

$$radial = \sqrt{(y_1 + y_2)^2 + \sin^2(TX_{steer})} \tag{11}$$

$$x = \sin(TX_{steer}) \tag{12}$$

$$y = y_1 + y_2 \tag{13}$$

$$z = \sqrt{1 - radial^2} \tag{14}$$

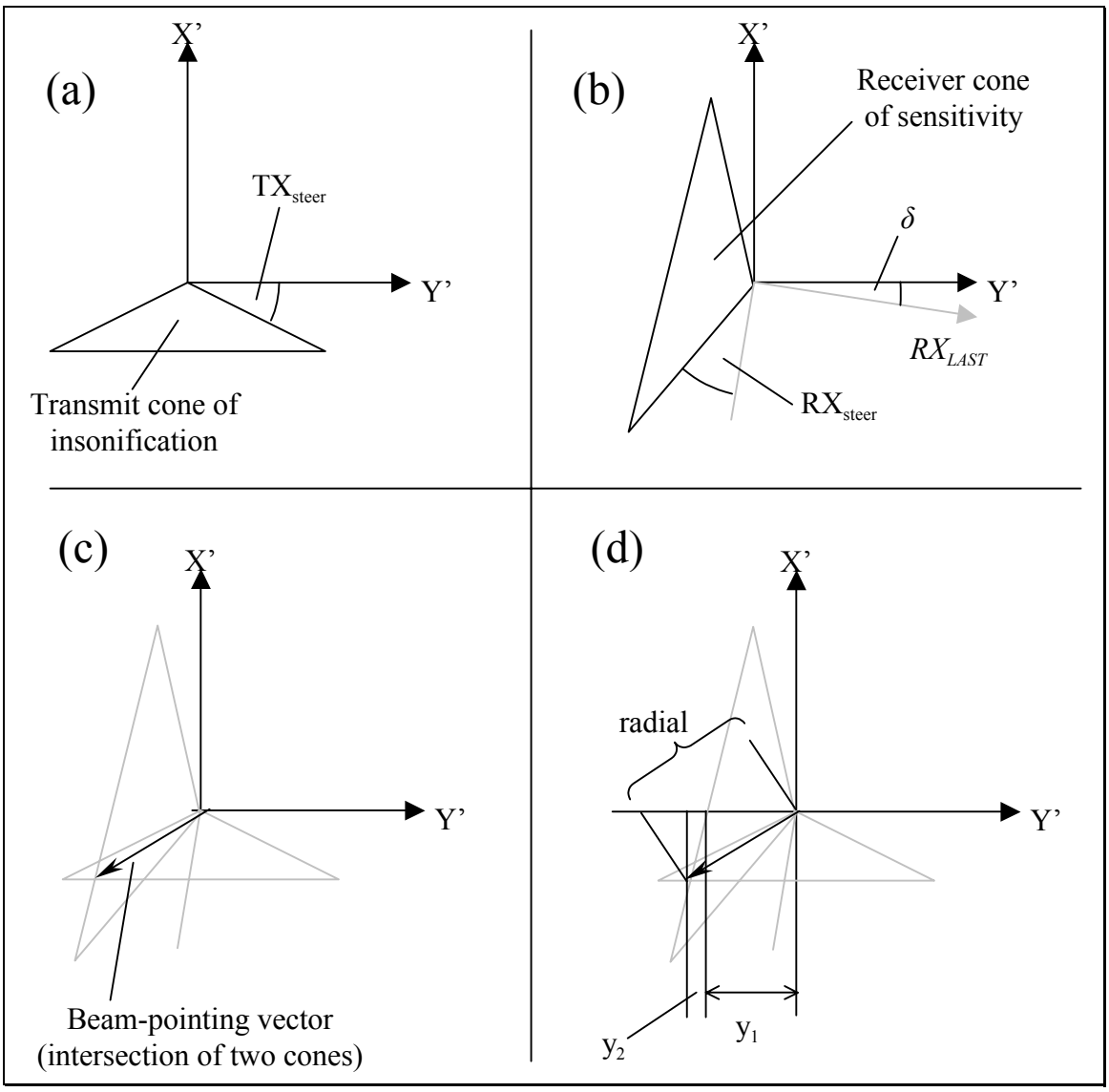

Figure 10. Geometry of transmit and receiver cone intersection. The beam-pointing vector lies on the intersection of the transmitter cone of insonification and the receiver cone of sensitivity, shown in (a) and (b) respectively with the intersection shown in (c). Image (d) demonstrates the geometry used to derive the beam-pointing vector coordinates.

The beam-pointing vector is then rotated into the local astronomical with a rotation matrix that contains the vectors of the primed-coordinate system as its rows:

$$\overrightarrow{BV} = \begin{bmatrix} X'_x & X'_y & X'_z \\ Y'_x & Y'_y & Y'_z \\ Z'_x & Z'_y & Z'_z \end{bmatrix} \cdot \overrightarrow{BV}_{prime} \qquad (15)$$

The beam azimuth and depression angle are then computed in the usual manner:

$$\alpha = \tan^{-1}\left(\frac{\overrightarrow{BV}_X}{\overrightarrow{BV}_Y}\right) \tag{16}$$

$$\beta = \tan^{-1}\left(\frac{\overrightarrow{BV}_Z}{\sqrt{\overrightarrow{BV}_X^2 + \overrightarrow{BV}_Y^2}}\right) \tag{17}$$

Finally, the azimuth is reduced to that of the heading at time of transmit.

$$\alpha_{relative} = \alpha - \alpha_{ship} \tag{18}$$

Complications

The process becomes difficult at this point for the EM300 as installed on the Amundsen due to the multi-sector transmitter arrangement that allows it to stabilize the transmit pattern for yaw, as shown in Figure 11. Multiple transmit sectors complicate the beam pointing vector determination in two ways: (1) each transmit sector has a unique transmit time, orientation and steering angle, and (2) the receive times are relative to the transmit time, so each receive beam must be associated with a unique transmit sector.

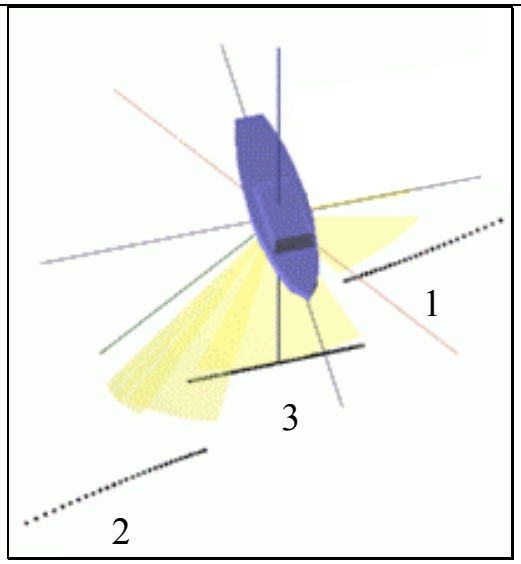

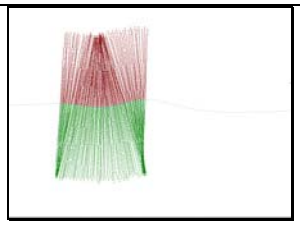

(a)

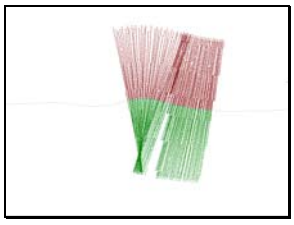

(b)

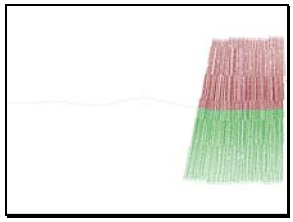

(c)

Figure 11. Usage of multiple transmit sectors to achieve yaw stabilization. With the EM120 and EM300, the outermost sectors are fired first, with the above image labeled in typical firing order. Application of yaw stabilization is demonstrated in the inset figures on the right. Inset (a) depicts 80 pings of soundings without yaw stabilization. The yaw stabilization is enabled halfway through (b) whereas all pings in (c) are yaw stabilized, highlighting the difference between both modes of operation [All images after Hughes Clarke, 2003].

The EM300 features several operational modes, each geared to a different range of water depths. The deepest mode features a long pulse length and low number of transmit sectors (due to signal extinction in the outer sectors) while the shallow modes use shorter pulse lengths [Kongsberg Simrad, n.d.]. The pertinent information for each mode is summarized in Table 3 below. Note that the sector boundaries and sector firing intervals were provided from the Kongsberg Simrad engineer who was onboard during the transit and that these values are not readily available to the user community. Personal communications with Kongsberg Simrad have confirmed the sector firing order to be outermost port sector, then outermost starboard, and so on, until the central sector is reached (as shown in Figure 11).

Table 3. EM300 operational modes.

Mode	Number of Sectors	Sector Boundaries (degrees) *positive=port, negative=starboard*	Sector Firing Interval (ms)

Extra-Deep	3	10.5, -10.5	15.51
Very-Deep	9	44,31.5,20.5,10.5 -10.0, -21.0, -31.5, -44.0	5.32
Deep	9	63.4, 44.7, 29.5, 18.4, -17.0, -31.0, -44.7, -63.5	5.32
Medium	3	60.0, -60.0	2.66
Shallow	3	60.0, -60.0	1.11
Very-Shallow	3	60.0, -60.0	1.11

To perform a beam re-pointing using data from the EM300, one must first determine the operational mode (stored in the run-time telegram, output by the transceiver). The operation mode dictates the number of sectors, in addition to the angular boundaries and time offsets between them. These values are then used to determine the times and orientations of the transmit and receive events. The procedure is as such:

1. For any given receive beam, one must determine its associated transmit sector using the depression angle stored in the depth telegram.
2. Determine the transmit time of the first sector (the time stamp of the depth telegram), then add the appropriate number of sector firing intervals to arrive at the transmit time of the receive beam's transmit sector. For example, referring to Figure 11, the third sector in Extra-Deep mode would be fired 30.02 ms after the first sector (2 x 15.51 ms = 30.02 ms). This offset is added to the depth telegram time stamp to arrive at the transmit time of the sector in question.
3. Compute the receive time by adding the receive beam's two-way travel time to the sector's transmit time.
4. Use the transmit and receive times to look up the orientation for both events and proceed as outlined in the procedure above.

Step 3: Perform raytrace

Raytracing algorithms allow for the modeling of the effect of refraction of a ray path given a depression angle, transducer depth and sound speed profile. The procedure

begins with an estimation of the transducer's depth. If significant along or across track lever arms exist between the vessels center of mass and the sonar, then the transducer draft is subjected to an induced heave when the ship pitches and/or rolls (in addition to the heave measured by the motion sensor). The induced heave may be accounted for by rotating the transducer's lever arms with the roll and pitch and using the resulting z component of the rotated vector (assuming that the reference point is at or near the center of mass of the vessel); this begins by rotating the lever-arms by a rotation matrix constructed using the orientation at the time of transmit, as in (19).

$$\overrightarrow{TX}_{rotated} = R_{orientation} \cdot \overrightarrow{TX}_{offsets} \tag{19}$$

The z-ordinate of the waterline and the heave at transmit are then applied to the z-ordinate of the rotated lever-arm vector, as in (20). This yields the actual vertical displacement between the reference point and the sonar.

$$draft_{TX} = Z_{TX_{rotated}} - Z_{waterline} + heave_{TX} \tag{20}$$

The same procedure is carried out for the receiver using its lever arms at orientation at the time of reception. The mean of the two computed drafts is then used as the starting point for the raytrace.

Step 4: Reduce to vessel reference point

The output of the raytrace is the total horizontal and vertical distance traveled during the ray's flight through the watercolumn. The vertical distance is added to the mean draft to yield the depth measurement (which need only be corrected for tide). The horizontal distance is broken into along-track and across-track components using the beam azimuth as derived during the cone intersection described earlier, as shown in (21) and (22).

$$across - track = d_{horizontal} \cdot \sin(\alpha_{relative}) \tag{21}$$

$$along - track = d_{horizontal} \cdot \cos(\alpha_{relative}) \tag{22}$$

The rotated transmitter lever-arms computed in (19) are added to these components in order to reference the sounding to the origin of the ship's coordinate system at the time of transmit.

Additional offsets must be added in the case that the reference point, or geometric center, of the sonar does not coincide with the acoustic center. The geometric center is typically the point on the transducer that would be considered the center when the vessel installation survey is performed. In practice, one must account for the additional lever arms and add them to the along-track, across-track and depth solutions. Examples include the EM1002 and EM3000D. In the case of the EM1002, all soundings must be reduced to the bottom of the barrel since the range measurement was made from the acoustic center of the subset of the receive barrel, as shown in Figure 12.

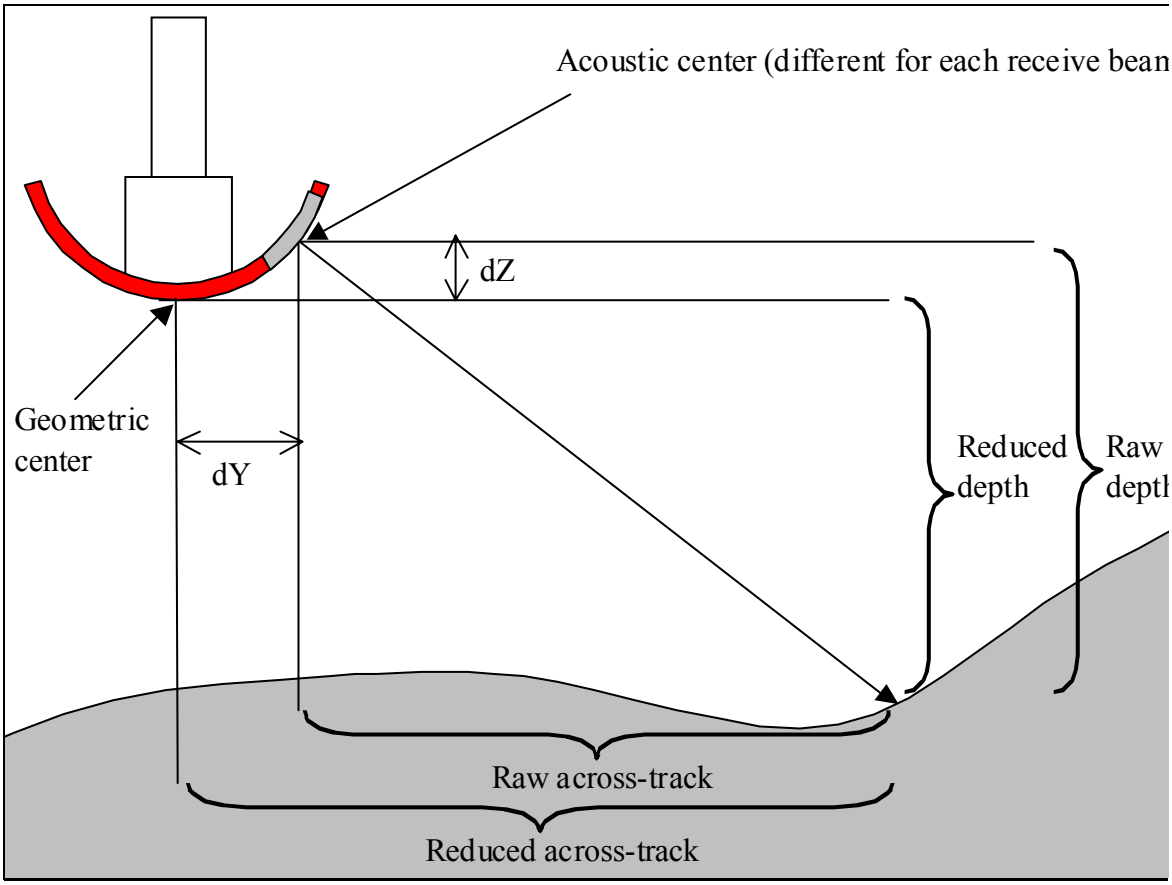

Figure 12. Application of offsets to reduce soundings from acoustic center of array to geometric center of the array for EM1002. The range measurement is made from the acoustic center, and once resolved into depth and across-track offsets, have dZ and dY applied to reduce the sounding to the geometric center of the array. Note that each receive beam has a unique dZ and dY offset.

A similar problem occurs with the EM3000D in that the transmitter and receiver arrays are offset from the geometric center of the transducer assembly. When the sonar heads are installed at their suggested mount angles, the small lever arms introduce depth

and across-track biases of a few centimeters. In both cases, the depth telegrams reported by the transceiver account for these additional offsets. If one were to reapply surface sound speed information then the appropriate offsets between the acoustic center and geometric center of the arrays must be computed and added.

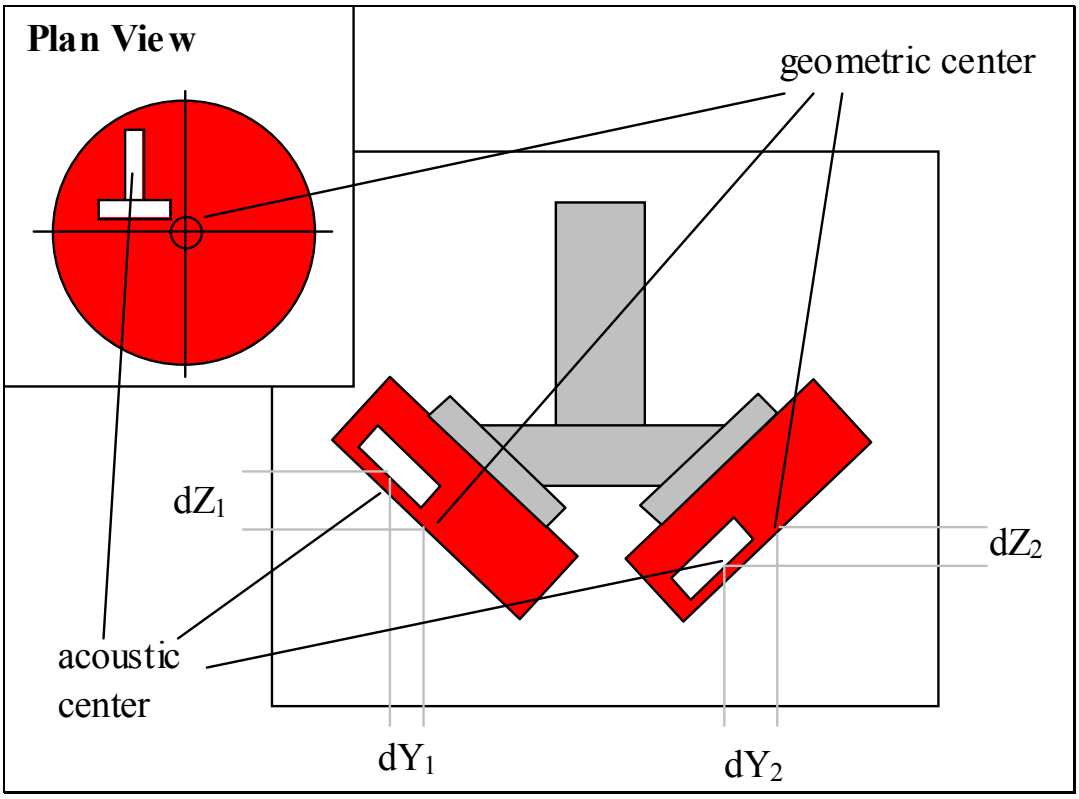

Figure 13. Internal offsets in typical EM3000D installation. The Mill's Cross is offset from the geometric center of the transducer as shown in the plan view. The center of the receiver array defines the acoustic center from which the range measurements are made. When the transducers are mounted in their typical configuration, the acoustic center of each transducer is offset from the geometric center of each array. Each transducer thus has an additional depth correction, dZ and across-track correction, dY. Unlike the EM1002, these values are shared by the receive beams associated with each transducer.

PRACTICAL APPLICATION: EM300

The above methodology was applied to a subset of the sections soundings outlined in Table 1. Statistical analysis of the application of surface sound speed is not possible due to a lack of overlapping survey lines. As such, accuracy checks are limited

to the comparison of soundings from swaths preceding and following the application of a beam pointing-angle correction. Similarly, it is difficult to assess the fitness of the methodology used for sound speed profile interpolation and application. At this point, visual analysis of the data is the only quality control that has been applied.

Surface Sound Speed

The sound speed artifacts shown in Figure 2 can be categorized based on their causes: either (1) the surface sound speed pump had failed, or (2) the pump was functioning, but its readings were ignored. Table 4 summarizes the required action in post-processing. Each of these cases is discussed further below.

Table 4. Proposed solutions for observed sound speed artifacts.

Artifact	Solution
A	Linearly interpolate surface sound speed from 1454 m/s to 1450 m/s, based on nearest valid data.
B	Linearly interpolate surface sound speed from 1435 m/s to 1432 m/s, based on nearest valid data.
D	Use logged surface sound speed value.
E	Use estimate of 1433 m/s based on nearest valid data.
F	Use logged surface sound speed value.
G	Use logged surface sound speed value.

Re-pointing based on estimates of correct surface sound speed

Sections A, B, and E fall within the category of soundings that must be corrected with estimates of surface sound speed. In the case of A and B, the operators noticed the failure and the last sound profile was used as the source of sound speed for beam steering purposes (the transceiver estimates the transducer's vertical position in the watercolumn and interpolates a sound speed value from a sound speed profile). Case E arose from an unnoticed pump failure, with the sound speed probe supplying the transceiver with grossly erroneous values. In post-processing, there was no choice but to re-point the beams based on an estimate of the correct surface sound speed for all three cases.

Section A

After examining the raw data in this section, it was confirmed that the probe was disabled and was not providing any data at all. The only option then is to re-point based on an estimate of the sound speed of when it became active. This was done for lines before and after activation, using 1449.6 m/s (instead of 1454.4 m/s). No large effect was noticed since the sound speed error was small. Nonetheless, the outer beam depths were corrected by about 2 meters (in approximately 650 meters of water, 0.3% water depth). A profile across the transition was prepared and is shown in Figure 14.

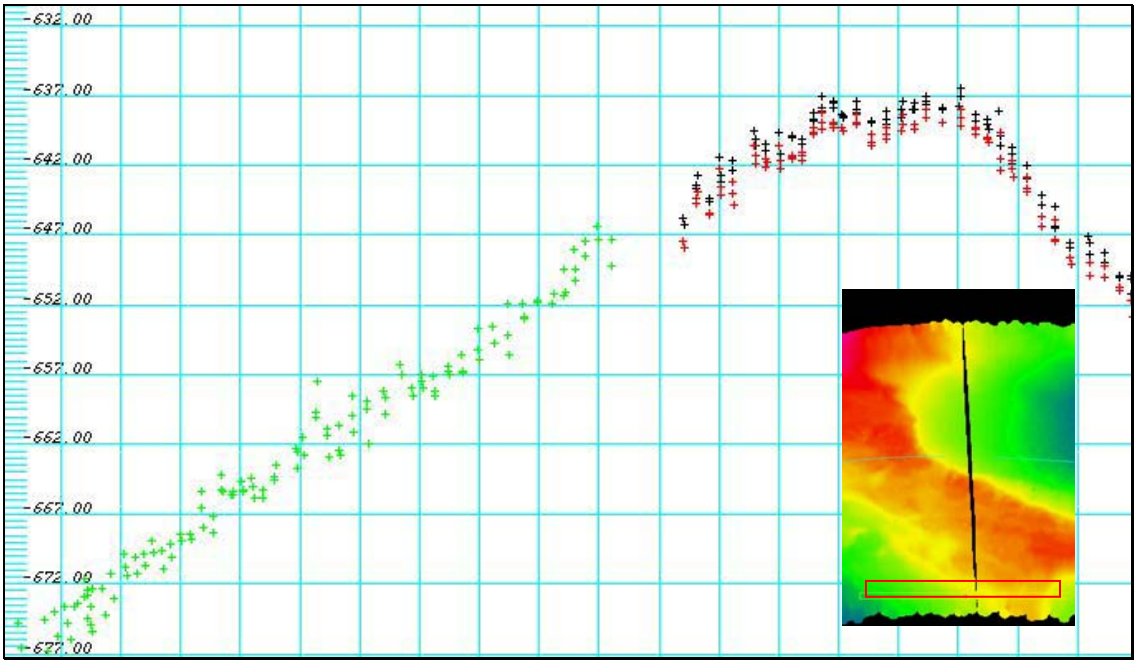

Figure 14. Re-pointing of Section A. Soundings are from outer beams of two survey lines, outlined in red in the inset image (colour-coded depth, ship track is from right to left). The surface sound speed probe was enabled during the transition between the two lines. Green soundings are from the survey line collected after the probe was enabled, while the red and black soundings represent the raw and corrected soundings, respectively, from the preceding survey line where the probe was disabled. Horizontal boxes are 100 meters wide.

Section B

Data from the surface sound probe became unusable due to heavy icebreaking, thus it was disabled and the transceiver was configured to use the sound speed from the last sound speed profile. The transition back to using the probe occurred shortly

afterwards. Data collected immediately before reactivation of the probe were re-pointed using an estimated surface sound speed of 1431.9 m/s (instead of 1454.4 m/s, which was applied by the transceiver). It is possible to re-point all of the soundings in this time period using an interpolated sound speed, however, the data are of extremely poor quality due to heavy icebreaking. Across-track plots of the soundings before and after the transition back to using the probe are shown in Figure 15.

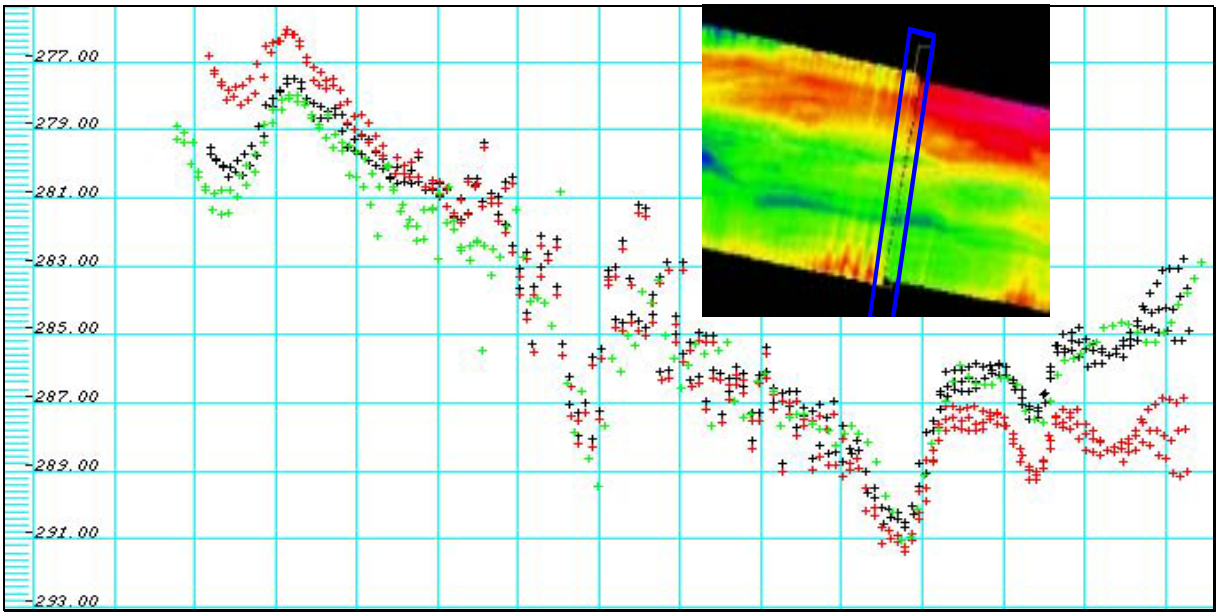

Figure 15. Across-track profile of raw and corrected data in Section B, bordering a transition from profile-based to probe-based surface sound speeds. Soundings are from three across-track profiles from the two survey lines bordering the transition (as shown in the inset colour coded depth image, ship track is from right to left). Green soundings are from the survey line collected after the probe was enabled, while the red and black soundings represent the raw and corrected soundings, respectively, from the preceding survey line where the probe was disabled. Note that the corrected soundings (black) agree well with the trend of the profile collected immediately after the probe was enabled (green). Horizontal boxes are 100 meters wide.

Section E

Data collected in Section E are characterized by a gross error in surface sound speed since the failure of the probe went unnoticed overnight with the probe reporting values of approximately 1480 m/s (whereas the true value was closer to 1430 m/s). Fortunately, a small area of overlap was found between lines collected before and after the probe failure. Subsets of the raw and corrected soundings are shown in Figures 16 and 17, respectively.

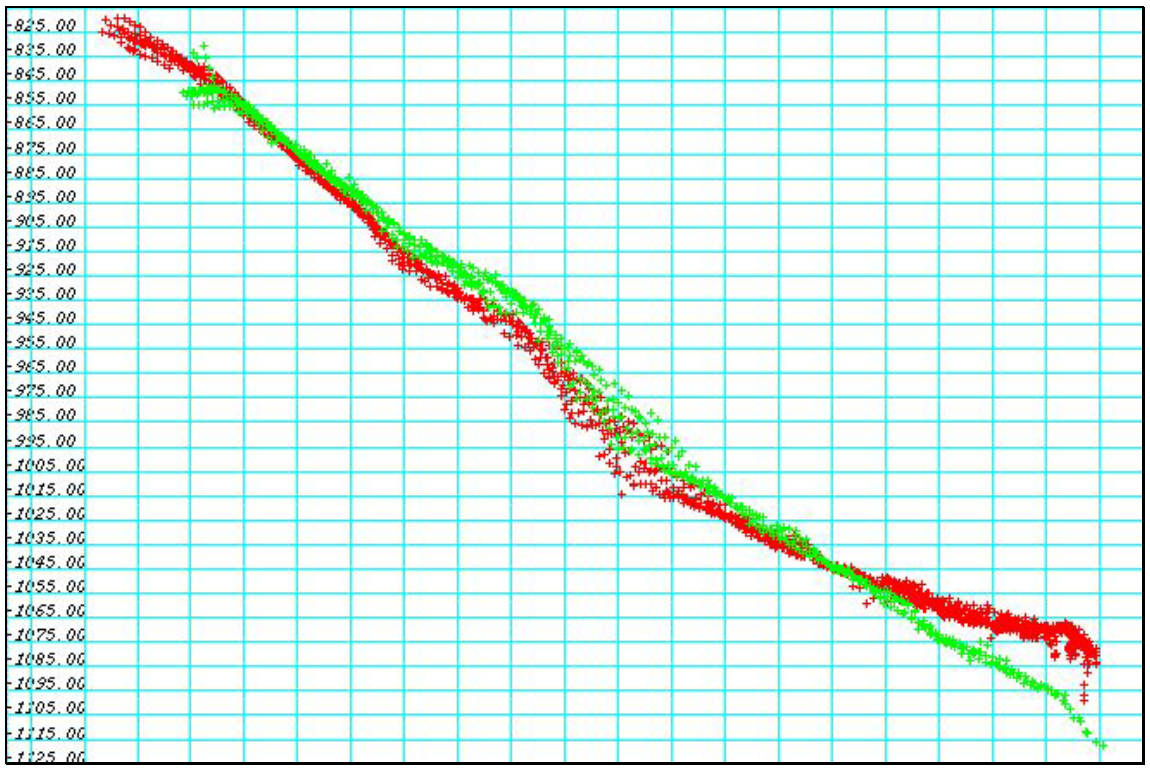

Figure 16. Raw soundings of Section E (green) compared to soundings from overlap line collected prior to sensor failure (red). Error approaches 1.4% of water depth in outer beams on right side of figure.

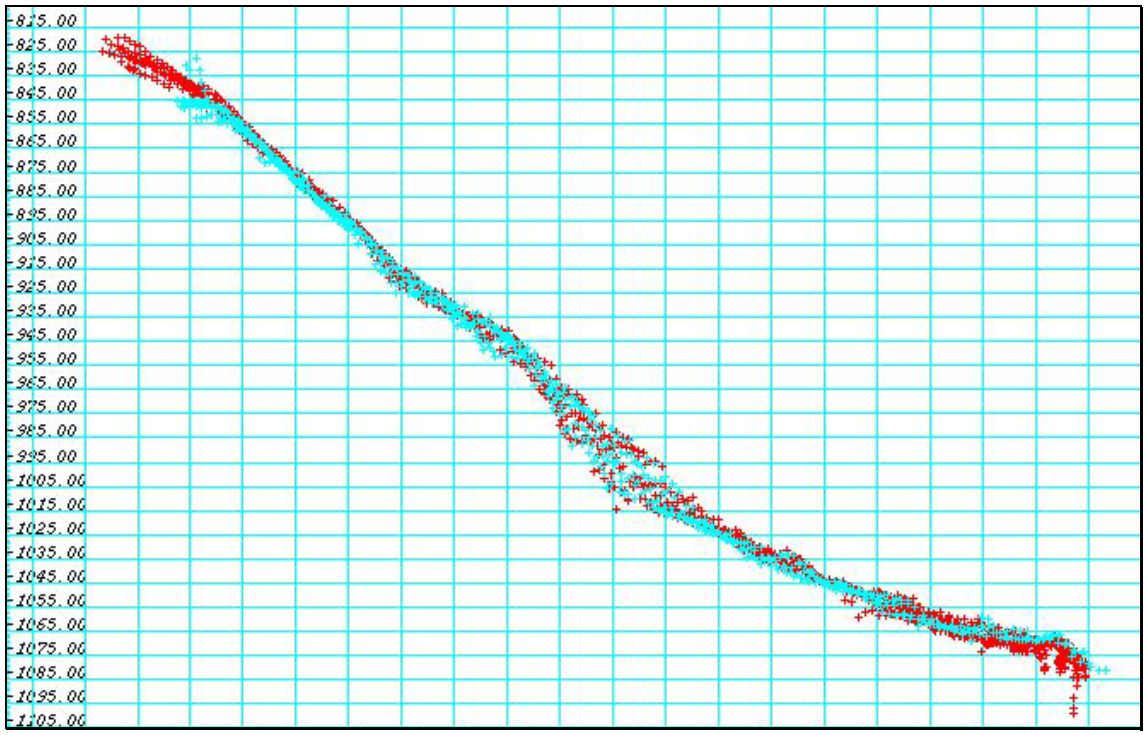

Figure 17. Corrected soundings (blue) of Section E compared to soundings from overlap line collected prior to sensor failure (red).

Re-pointing using sound speed probe data

Sections D, F, and G are incorrect because the surface sound speed probe values were ignored, either accidentally or intentionally, in favour of the value provided from the last sound speed profile (the grey arrows in Figure 18 indicate the sound speed profile value that was used instead of the value measured by the probe). Fortunately, the EM300 raw data format logs the surface sound speed probe values even if they are not applied. The data recorded during these periods are graphed in Figure 18; these values can clearly be used to correct the soundings in these sections.

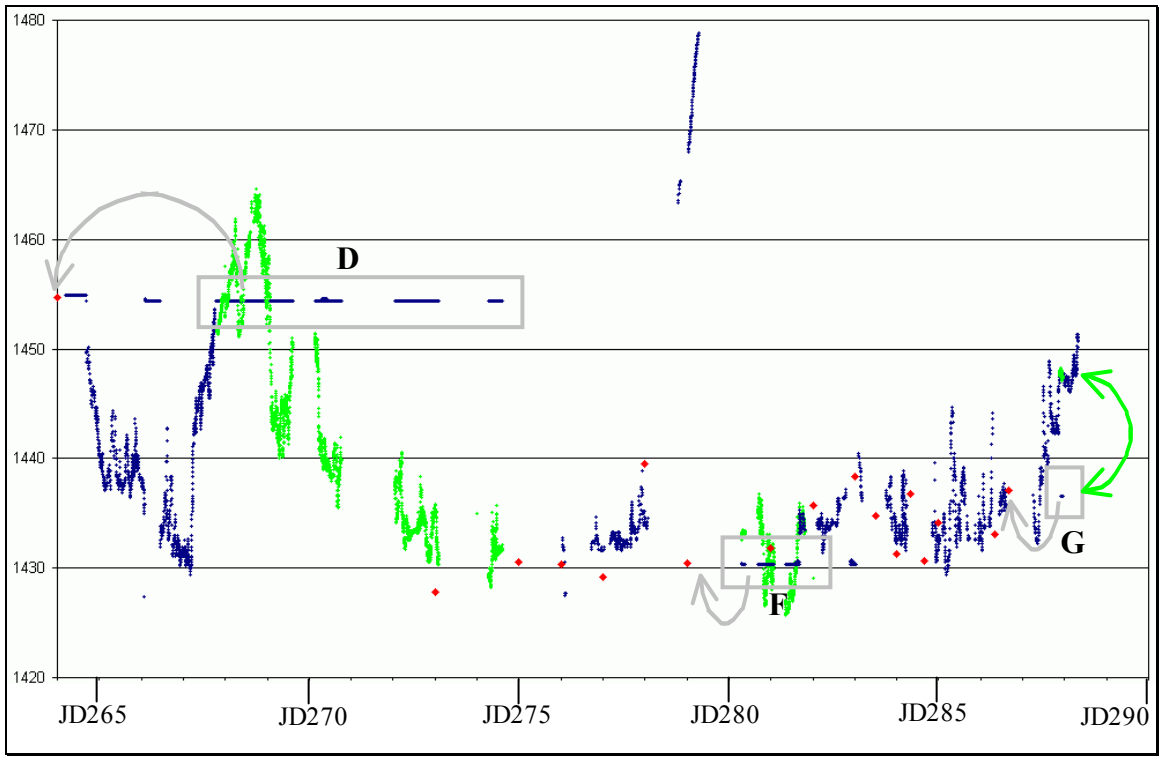

Figure 18. Comparison of applied sound speed vs. recorded sound speed. Applied values are shown in blue, recorded values are in green. Red samples are taken from transducer depth in sound speed profiles. Sections D, F, and G can be corrected using the actual recorded values.

Section D

After a system crash, the sound speed source for beamforming was accidentally set to use the last profile (1454.4 m/s) and unfortunately this setting remained unchanged for nearly a week. As shown in Figure 18, raw probe data were logged nonetheless and can be used to correct the soundings. A section of overlap was found in western Coronation Gulf (near Kugluktuk) between survey lines leading in and out of the gulf, collected several days apart. The soundings were corrected using an average probe reading of 1462.8 m/s with less than promising results. These poor results are likely due to the fact that the closest sound speed profiles are from Baffin Island (~1,600 km away) and the Amundsen Gulf (~400 km away).

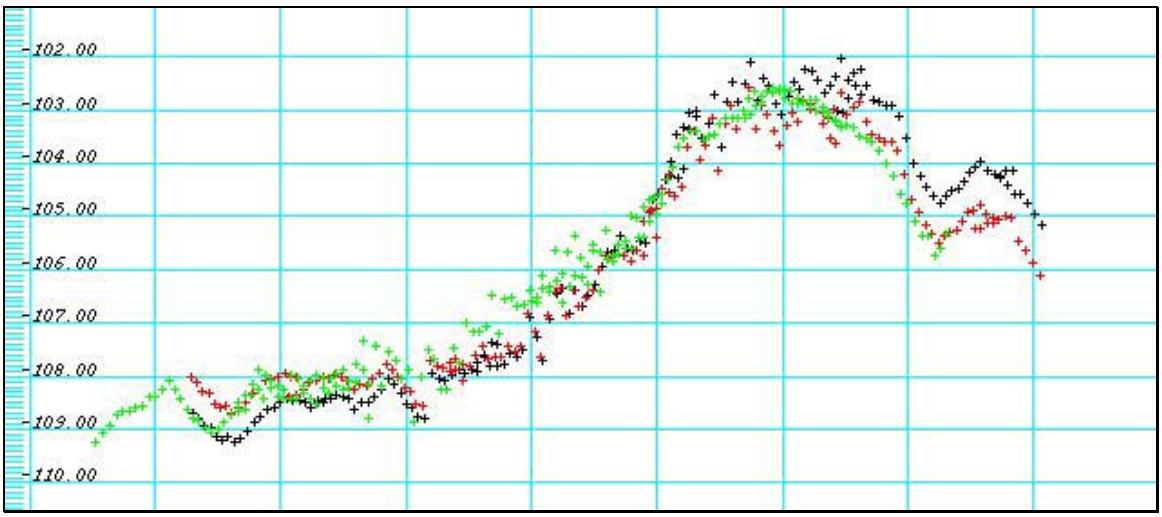

Figure 19. Re-pointing of soundings in Section D. The red and black soundings represent the raw and corrected soundings, respectively, whereas the green soundings are from a reciprocal survey line collected at the end of the transit while steaming back to Kugluktuk. The lack of agreement between the green and black soundings is likely due to the inapplicability of the sound speed profiles used to reduce the soundings.

Section F

The soundings in Section F were collected after the probe failure in Section E. The probe was repaired shortly after the failure was noticed, however, the operator was not informed of this for quite some time (the system logged the probe data regardless, these values were used to correct the soundings in post-processing). Unfortunately, no areas of independent soundings exist to verify the accuracy of the re-pointed soundings.

A sample of the raw and corrected soundings is presented in Figure 20. Error magnitude in the outer beams approached 0.5% of water depth, demonstrating that the error in sound speed (approximately 5 m/s) can quickly reduce the accuracy of the outer beams.

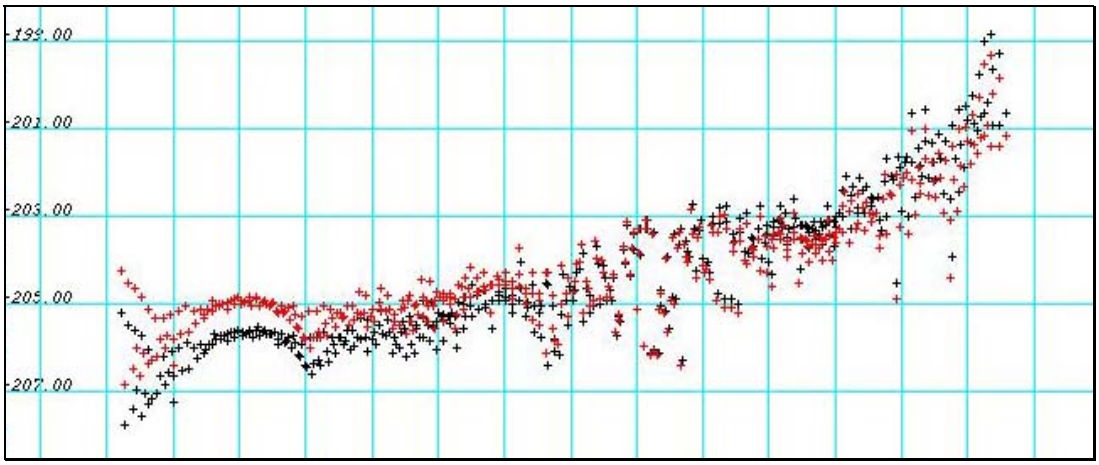

Figure 20. Re-pointing of soundings in Section F, with red and black representing the raw and corrected soundings, respectively. No area of overlap with other survey lines is available for comparison.

Section G

In this case, the operator momentarily toggled between using the probe and the last profile as the source of sound speed for beam steering (the last sound speed profile collected was a few hundred kilometers away). After a brief interlude of using the profile as the source, the operator switched back to using the probe. The soundings during this time period must be corrected based on the logged probe values since a surface sound speed error of approximately 11 m/s was introduced during this short time (introducing a depth error of approximately 1.25% of water depth in the outer beams). The transition between probe sound speed and profile sound speed is shown in Figure 21, with the raw and corrected soundings contrasted against the ping immediately preceding the transition.

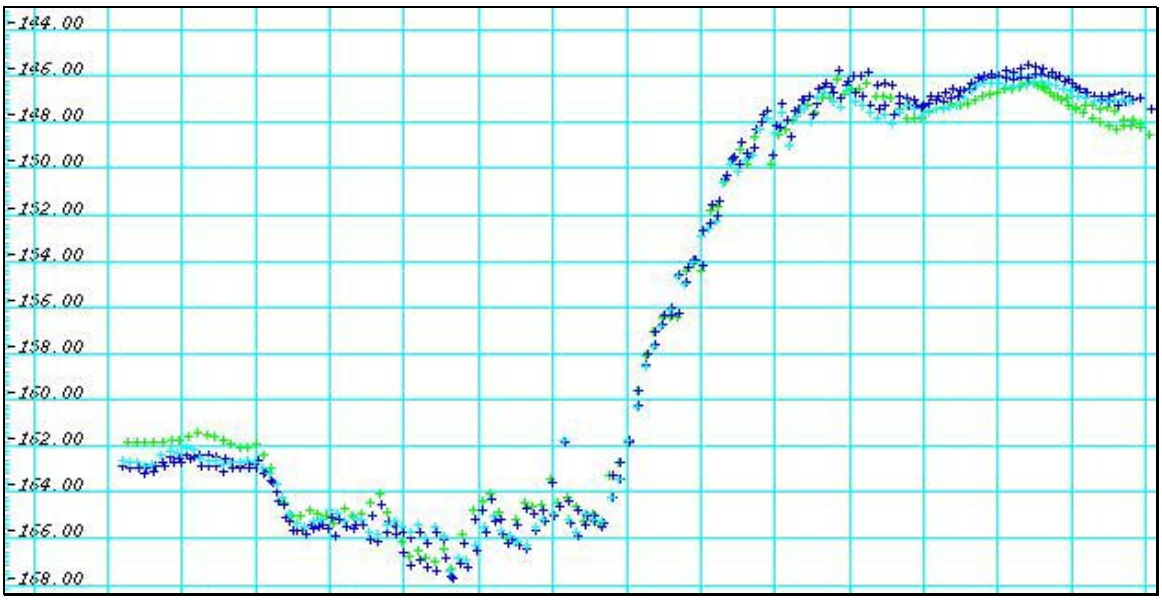

Figure 21. Re-pointing soundings in Section G. Data are from 2 swaths surrounding the transition from probe to profile as the source of sound speed for beam steering. Soundings in light blue were collected prior to the transition and are considered correct. Green soundings were collected using the erroneous sound speed value from the profile with the dark blue soundings being the corrected versions of the green. The re-pointing procedure has removed depth errors of 1.25% of water depth in the outer beams of the green soundings.

Sound Speed Profiles

When faced with near-continuous sound speed profiles, the standard OMG technique is to use interpolation between the profiles to allow for a better approximation of the underlying oceanographic processes that are driving the changes in the water column [Hughes Clarke, et al., 2000]. Hughes Clarke concluded that there is nothing to be gained through time interpolation if the profile sampling interval is less than the time scale of the oceanographic processes; this obviously applies to the transit through the Northwest Passage given the 7-day interval between the collection of sound speed profiles. Figure 22 demonstrates the inadequacy of the time-interpolation technique for the transit data (JD264 to JD273).

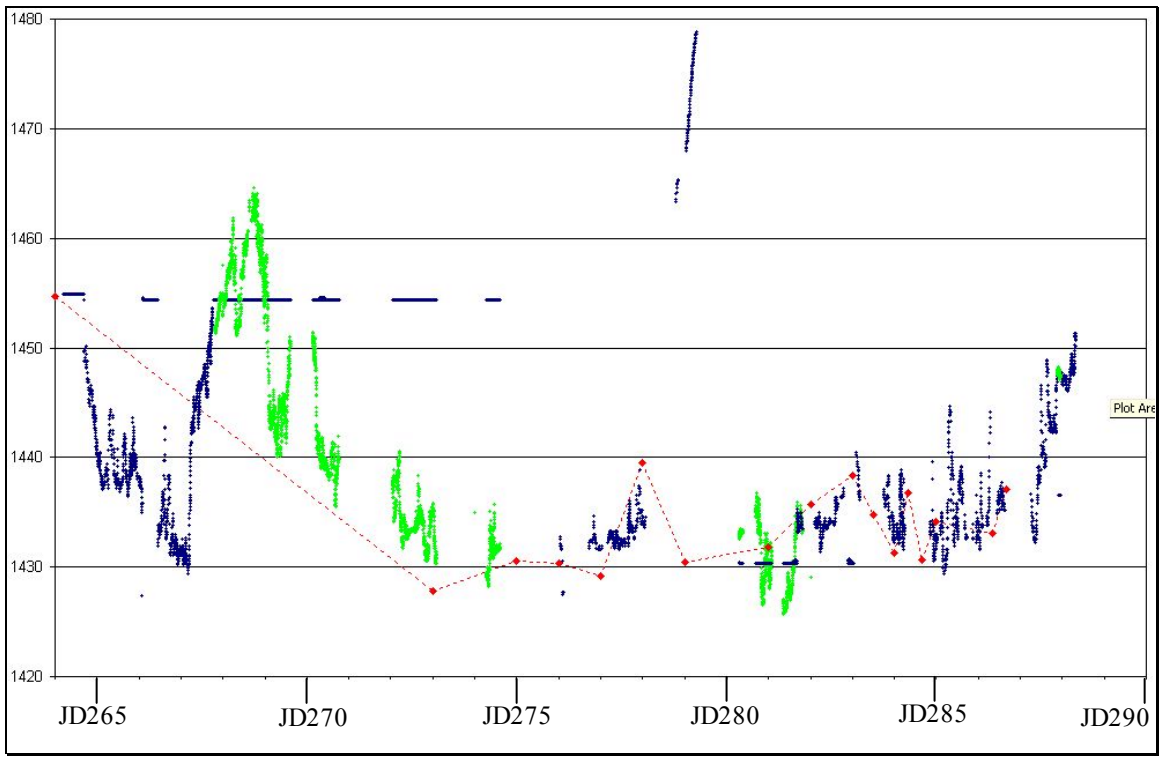

Figure 22. Interpolation of surface sound speed between profiles. Surface sound speed probe values are shown in blue and green (blue is the applied value, green is the measured value which may have been ignored by the transceiver). Red values represent the sound speed near the transducer depth from sound speed profiles collected during the transit. Using the time-interpolation technique between sound speed profiles would introduce surface sound speeds into the interpolated profiles (represented by the red-dashed line); this obviously fails to capture the surface speed variation during the transit through the Passage (JD264-JD275) though it may prove viable though in the western portion of the transit (JD275+) due to the relatively high sampling frequency of sound speed profiles.

The technique is perhaps viable for the data collected in the Amundsen Gulf and Beaufort Sea, though the sampling interval ranged from several hours to once per day (yielding 16 profiles in as many days). Given that the ship was constantly steaming through intermittent ice, the variability at the sea surface due to freeze/thaw of ice is likely to negate the advantages of time-interpolation of watercolumns. The time-interpolation technique was used regardless since the sound velocity profiles were provided several hours after the collection (up to a day in some cases) and had to be propagated backwards in time to the point of their collection in post-processing. Even so, the only time-tagging information on the sound speed profiles was the date of collection. Until the raw files can be acquired on the next visit to the ship, we are left with estimates

of the time of collection for each profile (which is why most of the profiles occur at the midnight mark in the time series graphs such as Figure 22). If time interpolation techniques are to be used, then due care must be taken to note the collection time of the profile independently.

Further problems are encountered when attempting to interpolate between a profile collected in the Beaufort Sea (extending to 1200 meters) and another profile collected on the Mackenzie Shelf (extending to only a few hundred meters). This becomes an issue when steaming down the shelf, since the last available profile proves to be too shoal. The transceiver circumvents this problem by artificially extending all profiles to 12,000 meters based on open ocean models, however, these extensions likely do not apply to the Arctic Ocean, whose vertical sound speed profile is dominated by salinity and not temperature [Boilard, 1993]. Clearly, some improvement can be made in post-processing since the profiles applied by the transceiver would be significantly in error on downward runs of slopes. The approach taken in this study was to artificially extend all profiles using the 1200-meter profile collected in the Beaufort Sea. This is not unreasonable since the majority of the profiles agree remarkably well below 100 meters, as shown in Figure 23. The most significant exception was a profile collected in the Mackenzie Trough, extending to some 900 meters (visible as the profile extending to 1455 m/s at the surface). Despite its deviation from the norm in the upper 100 meters, it converges to the deep Beaufort profile at a depth of approximately 400 meters.

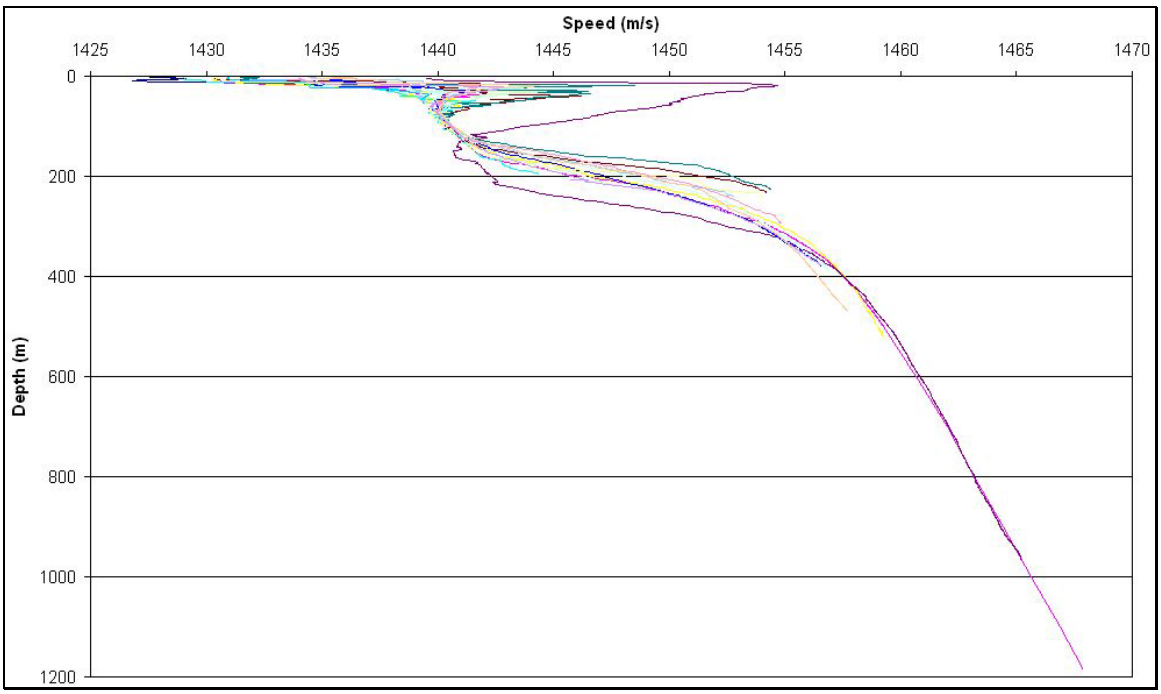

Figure 23. Graph of 16 sound speed profiles collected in Amundsen Gulf and Beaufort Sea between JD273 and JD287. Deep profiles are from Beaufort Sea and Mackenzie Trough while all others are on Mackenzie shelf and in Amundsen Gulf (refer to Figure 3 for geographic distribution of profiles). The majority of the profiles agree below 100 meters depth with most of the variation occurring in the top 25 meters of the watercolumn.

A systematic evaluation of this approach to the application of sound speed profiles has yet to be done, however, it is the subject of ongoing research in the OMG in preparation for the 2004 field season onboard the Amundsen. In any case, it is difficult to assess the suitability of sound profile post-processing given that very little overlap is achieved during transit type surveys. Part of the scientific research work onboard the Amundsen is being done to better understand the oceanography of the Arctic Archipelago; it is hoped that the new findings that arise will aid in the intelligent application of sound speed profiles.

CONCLUSION AND RECOMMENDATIONS

It has been demonstrated in this paper that it is possible to correct soundings corrupted by incorrect surface sound speed values in post-processing as long as the

appropriate information is retained in the raw data stream. Several instances of faulty surface sound speed were re-processed with promising results, even in the face of gross sound speed errors applied by the transceiver in real-time. Though this process has improved the accuracy of the data collected by the Amundsen, the lack of sound speed profiles is likely the limiting factor in the overall accuracy of all the soundings, let alone those that were re-processed for surface sound speed errors. This technique can be extended to other sonars which store the above information in their data format and whose operation is well understood (e.g. multi-sector transmit sectors, internal sonar offsets).

Four main recommendations can be made based on the findings in this work including extra experimental test to verify the accuracy of the proposed method in this work and procedural changes that should assist and/or minimize the amount of post-processing.

1. A rigorous testing exercise should be planned in which a small patch is surveyed using the sound probe to generate a reference surface. Cross-lines can then be run with intentionally incorrect surface sound speed values being entered into the system to observe the effect and to test the procedure developed in this work.
2. Much of the post-processing required detective work to determine the cause of spurious sound speed sensor values since no logs were kept during the transit (due to the "shakedown" nature of the cruise, many other things were overlooked as well). A sound speed log should be kept in which the following should be noted:
    a. Surface sound speed values reported from the probe, entered a few times daily.
    b. Reasons for surface sound speed probe failure and action taken.
    c. Notation on circumstances surrounding any change in the source of surface sound speed.
    d. Time and position of sound speed profiles, including time that they were uploaded to the EM300 transceiver.
3. Daily procedures should include checking the status of the sound speed probe and comparing it to any real-time sensors available (perhaps other scientists onboard have real-time salinity or temperature sensors). In the highly likely case of

another probe failure, it is much more appropriate to enter a user-specified value from the logbook as opposed to using the last sound speed profile (which may be grossly incorrect). Using a realistic estimate of the surface sound speed may reduce the amount of post-processing.

4. In the interest of reducing the amount of post-processing, all efforts should be made to ensure timely delivery of sound speed profiles from CTD rosette casts to the EM300 operator. Currently, profiles from casts must be calibrated by the CTD rosette operator (with this understandably being left until all daily oceanographic equipment deployments have been finished). It may be wise to invest time in training EM300 operators to calibrate the CTD files independently of the CTD rosette operations such that the profile may be entered into the EM300 transceiver as soon as possible.

REFERENCES

Boilard, Y. (1993). Environmental Guide for Maritime Operations in the Canadian Arctic Archipelago. Thesis submitted for M.Sc. Royal Roads Military College, Aug. 1993. Victoria, British Columbia.

Hughes Clarke, Lamplugh, M., and E. Kammerer (2000). Integration of near-continuous sound speed profile information. Canadian Hydrographic conference 2000, Proceedings, CDROM.

Hughes Clarke, J.E. (2003). GGE 3353 Lecture Notes. Department of Geodesy and Geomatics Engineering, University of New Brunswick, Fredericton, New Brunswick.

Kongsberg Simrad (n.d.). Simrad EM300 Multibeam Echo Sounder. Product Specification, Horten, Norway.